Charge transport in columnar mesophases of carbazole macrocycles

Thorsten Vehoff, Björn Baumeier,[a] and Denis Andrienko[b]
Max Planck Institute for Polymer Research, Ackermannweg 10, D-55128 Mainz, Germany

(Received 1 September 2010; accepted 22 September 2010; published online 7 October 2010)

Charge transport properties of a columnar mesophase of carbazole macrocycles are analyzed. Realistic morphologies are sampled using all-atom molecular dynamics simulations while charge transport is simulated using the kinetic Monte Carlo method with transfer rates obtained from the high temperature nonadiabatic limit of Marcus theory. It is shown that the molecular design with side chains pointing inside the macrocycle allows close approach between molecules of neighboring columns, thus enabling three-dimensional transport and helping to circumvent charge trapping on structural defects. © *2010 American Institute of Physics*. [doi:10.1063/1.3501360]

I. INTRODUCTION

Optimal photogeneration of excitons, their fast separation into electrons and holes, and the swift transport of free charge carriers to the electrodes are the determining factors for the design of solar cells with high power conversion efficiency.[1,2] In organic semiconductors, weak intermolecular forces and low dielectric constants lead to localized and strongly bound electron-hole pairs (excitons). Neither thermal energy, nor the electric field provided by the electrode workfunctions, is strong enough to dissociate these excitons.

To remedy the situation, an electron donor (D) and electron acceptor (A) mixture can be used. The idea behind such a heterojunction concept is to have different electron affinities and ionization potentials of two materials. At a DA interface, the resulting potentials favor exciton dissociation: the electrons will be accepted by the material with the larger electron affinity, while the hole will be accepted by the material with lower ionization potential. In an efficient device, the difference in the potential energy should be larger than the exciton binding energy and excitons should be formed within the diffusion length of the DA interface. The exciton diffusion lengths in organic materials are, however, much shorter than the absorption depth of the film, which limits the width of the efficient light-harvesting layer. To avoid this bottleneck, the donor and acceptor materials are blended together.[3] The domain size in such a bulk heterojunction must be of the order of the exciton diffusion length, in which case there is a DA interface in the proximity of every generated exciton. Hence, dissociation and charge generation take place everywhere within the active layer. In order to minimize the carrier transport time and to reduce the probability of back electron transfer, efficient exciton dissociation shall be complemented by straight pathways to electrodes for both types of charge carriers. The immediate implication is that *ordered* bulk heterojunctions are required, with, for example, stripe-like or cylindrical domains spanning the whole cell.[4]

In spite of their well-defined requirements, the design of such compounds for ordered bulk heterojunctions is rather complicated.[5–8] Several types of organic semiconductors, capable of self-assembly on a nanoscale, have been evaluated, among them columnar discotic liquid crystals (LCs).[9–12] These form conductive columnar structures with flat conjugated π-systems surrounded by insulating side chains. The main disadvantages of such columnar architectures are inefficient exciton dissociation due to insulating side chains between donor and acceptor and the one-dimensional nature of the transport. In one dimension, charge carrier mobility is highly sensitive to the presence of defects, since a single disruption of the connectivity, caused either by static disorder or intrinsic assembly defects, can effectively inhibit charge transport.[13–16]

Both problems can be addressed by using a so-called donor-bridge-acceptor concept, where donor and acceptor are covalently linked. The bridge constrains the DA separation and helps to control charge and energy transfer efficiency between the donor and acceptor. This concept has recently been used in donor-bridge-acceptor-bridge block copolymers.[17,18] In discotic LCs, an analog would be a ring-core structure with the core formed of a donor material, while the ring is made of an acceptor, or vice versa. If such a molecule assembles into a columnar superstructure, it gives rise to separate pathways for holes and electrons. In this context, the synthesis of a π-conjugated macrocycle consisting of polycarbazole has been reported.[19] In the bulk, the macrocycles form columns arranged on a hexagonal lattice and the cavity inside may be filled with graphene-like molecules.[20]

In this paper, we will demonstrate that an additional advantage of the macrocycle-based architecture is that the side chains can point inward, allowing for a substantially reduced intercolumnar separation in the assembled superstructures. This leads to rather high electronic couplings between molecules in neighboring columns. A resulting three-dimensional charge-percolating network helps to circumvent problems with structural defects, which is crucial for efficient charge transport.

[a]Electronic mail: baumeier@mpip-mainz.mpg.de.
[b]Electronic mail: denis.andrienko@mpip-mainz.mpg.de.

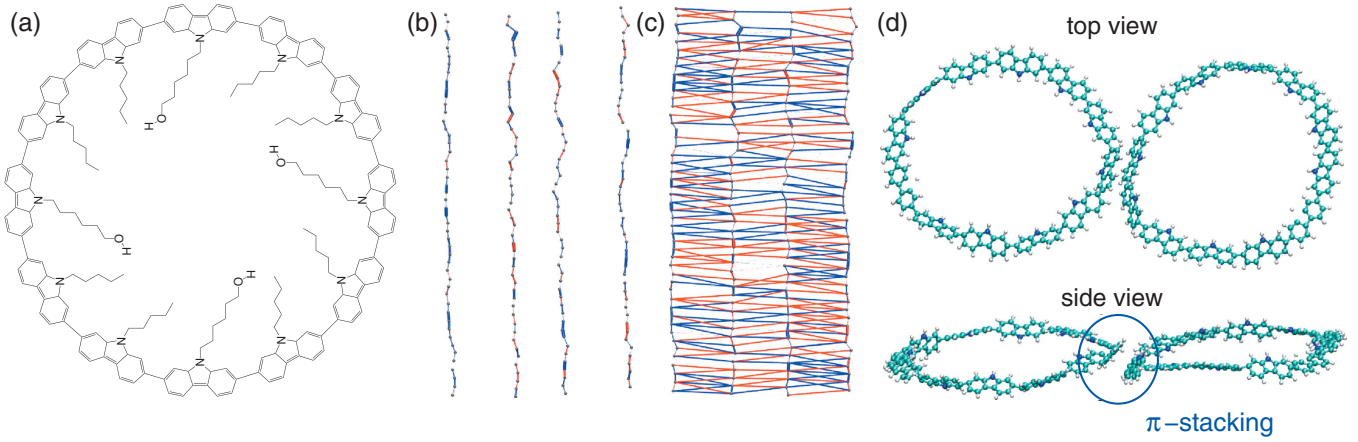

FIG. 1. (a) Chemical structure of the modeled carbazole macrocycle. Connectivity graphs (side view) for one-dimensional (b) and three-dimensional (c) transport for a model with a fully conjugated macrocycle. Grey spheres represent the centers of mass of each macrocycle. The width of the bond is proportional to the transfer integral, the color represents the sign with blue being positive and red negative. (d) Exemplary conformation of neighboring macrocycles perpendicular to the columnar stacking showing high electronic coupling.

II. MOLECULAR DYNAMICS SIMULATIONS

The studied chemical structure of a single macrocycle is shown in Fig. 1(a). In this ideal configuration, the molecule has a fourfold rotational symmetry due to the presence of the four OH side chains.

Molecular dynamics (MD) simulations were performed using the GROMACS package.[21] The OPLS-based force-field was used with the torsional potential between adjacent monomer units parametrized as described in Ref. 22. The initial morphology was prepared based on x-ray experiments.[19] According to experimental data, the individual columns are arranged on a hexagonal lattice with a packing distance of 4.7 nm. Within a column, the intermolecular spacing is 0.4 nm, with neighboring molecules rotated at an angle of 30° with respect to each other, leading to a helical pitch with a correlation of every fourth macrocycle.

In our simulations, we considered a system of $4\times4\times48$ carbazole macrocycles, i.e., 16 columns of 48 molecules each, with periodic boundary conditions. A time step of 1 fs was used. The runs employed a smooth particle mesh Ewald algorithm[23] with explicit treatment up to 1.2 nm to calculate electrostatics and a cut-off of 1.2 nm for van der Waals interactions. Initial velocities were generated from a Boltzmann distribution at 300 K. The NPT equilibration run lasted 2.4 ns with Berendsen pressure coupling and the velocity rescaling including stochastic velocity rescaling thermostat.[24] During equilibration, the intercolumnar separation was reduced to about 3.7 nm, while the distance between neighboring molecules within a column increased to 0.45 ± 0.02 nm. Following the NPT equilibration, we performed an NVT equilibration of 1 ns using the velocity rescaling thermostat. The final NVT production run of 20 ps was used to save configurations every 20 fs.

Note that the carbazole macrocycles reported in Ref. 19 were prepared on highly ordered pyrolytic graphite, while in the simulations we were interested in a columnar mesophase. Additionally, the branched alkyl side chains reported by Jung *et al.*[19] were substituted by linear chains of four carbons in length which reduces steric hindrance. This explains the differences between the experimental and simulated morphologies. Synthesis-wise, shortening of side chains is a straightforward procedure, which also allows for the insertion of a central π-system, such as a graphene molecule, to form a donor-acceptor system.[20]

III. HOLE TRANSPORT

Kinetic Monte Carlo (KMC) simulations were performed based on the MD configurations using the VOTCA package.[25] An important detail in these simulations is the definition of charge transport units or conjugated segments.[26] In the following, we will consider two cases: (a) that the whole molecule is conjugated and the charge carrier is delocalized over the full cycle, and (b) that the charge carrier is localized on a single monomer unit. In case (a), the diabatic states for the calculation of the transfer integrals for hole transport are then constructed based on the highest occupied molecular orbital of an optimized macrocycle. To account for the changes of the dihedral angle between neighboring monomer segments, the orbitals of the optimized macrocycle are rotated according to the respective orientation of the monomer segments. Hopping rates are calculated using nonadiabatic high temperature Marcus theory,[27]

$$\omega_{ij}=\frac{J_{ij}^2}{\hbar}\sqrt{\frac{\pi}{\lambda k_{\mathrm{B}}T}}\exp\left[-\frac{(\Delta G_{ij}-\lambda)^2}{4\lambda k_{\mathrm{B}}T}\right], \tag{1}$$

where λ is the reorganization energy, J_{ij} is the transfer integral, ΔG_{ij} is the free energy difference between initial and final states, and $k_{\mathrm{B}}T$ ($T=300$ K) is the thermal energy.

In case (b), we assume that two monomer segments α and β are interconnected by additional intramolecular charge transfer rates, modeled using an expression from transition state theory,

$$\nu_{\alpha\beta}=\nu_0\exp\left[-\frac{(\Delta G_{\alpha\beta}-\Lambda)^2}{4\Lambda k_{\mathrm{B}}T}-\frac{|J_{\alpha\beta}^{\mathrm{intra}}|}{k_{\mathrm{B}}T}\right]. \tag{2}$$

Here, ν_0 is a prefactor related to the frequency of the promoting mode and the relevant Franck–Condon factor.[28] In

accordance with Ref. 26, we chose a value of $\nu_0 = 10^{15}$ s^{-1}, ensuring that intrachain rates are fast enough so that global charge transport is dominated by interchain rates. Λ is the reorganization energy of a single carbazole monomer, while the intramolecular transfer integral is approximated by $J_{\alpha\beta}^{\text{intra}} = J_0 \cos \Psi_{\alpha\beta}$, where $\Psi_{\alpha\beta}$ is the torsional angle between neighboring monomers and J_0 is set to 0.1 eV.

Density-functional theory (DFT) calculations were performed with the GAUSSIAN03 package[29] to obtain the reorganization energy for a single molecule in vacuum using the B3LYP hybrid functional[30] and a 6-311G(d,p) basis set, yielding $\lambda = 0.06$ eV for the full macrocycle and $\Lambda = 0.10$ eV for the single carbazole monomer. Transfer integrals between neighboring molecules are evaluated using a method based on Zerner's intermediate neglect of differential overlap as implemented in the Molecular orbital overlap package.[31] Selected results have been checked against transfer integrals obtained from DFT-based calculations using the dimer projection method.[32] No significant differences could be observed.

The free energy difference has two contributions, $\Delta G_{ij} = \Delta G_{ij}^{\text{ext}} + \Delta G_{ij}^{\text{estat}}$. $\Delta G_{ij}^{\text{ext}} = e\boldsymbol{E}\boldsymbol{r}_{ij}$ is due to an externally applied electric field $\boldsymbol{E}$, where e is the elementary charge and $\boldsymbol{r}_{ij}$ the vector connecting the two sites i and j. The externally applied electric field was chosen to have a magnitude of $E = 10^7$ V/m throughout and is always aligned parallel to the direction of transport, i.e., in x-, y-, or z-direction, respectively. $\Delta G_{ij}^{\text{estat}}$ arises from the different electrostatic interaction energies depending on the localization site of the charge carrier. For a carbazole monomer in vacuum, DFT calculations yield a dipole moment of ~ 2 D pointing into the direction of the nitrogen atom. In the ideal macrocycle, the dipole moment is only 0.03 D since monomer dipoles facing toward the center of the cycle compensate each other. However, due to changes of the conformation of the molecules in the equilibrated morphology, one cannot assume *a priori* that the effect of electrostatic disorder in $\Delta G_{ij}^{\text{estat}}$ is negligible. The electrostatic site energy difference is computed according to Ref. 15. The required partial atomic charges are determined using the CHELPG method for neutral and anionic state of a carbazole macrocycle in vacuum.

For both conjugation models, absolute values of transfer integrals range from 10^{-1} to 10^{-8} eV. Some of the values for J are comparable in magnitude to the respective reorganization energy, 0.06 eV. This indicates that the assumption of a site localized charge carrier as described in the hopping regime may not be fully valid in this case. However, we have recently shown[33] that even in such a situation, mobilities determined using Marcus theory are comparable to those obtained, e.g., from semiclassical dynamics calculations. We assume that the same holds for the carbazole macrocycle. Additionally, there is a significant amount of disorder present in the columns, which further localizes charge carriers.

Connectivity graphs as in Figs. 1(b) and 1(c) show the strength of the intermolecular coupling between hopping sites based on the magnitude of the individual transfer integrals and reveal the topology of the transporting network. The fact that the side chains of the carbazole macrocycles face into the cavity allows a close approach between cycles of neighboring columns. In contrast to columnar assemblies of discotic liquid crystals, for instance, this results in distinct electronic coupling also perpendicular to the stacking direction of the columns. To scrutinize the effect of this coupling, we compare one-dimensional transport, i.e., transport only along the stacking direction, to three-dimensional transport. The resulting connectivity graphs [see Figs. 1(b) and 1(c)] not only show a much denser network in 3D but also reveal that intercolumnar coupling is sometimes comparable in magnitude to the coupling within the columns. The highest intercolumnar transfer integrals are found when the closest monomer segments of neighboring macrocycles rotate in such a way that they align almost cofacially, as is shown in Fig. 1(d).

TABLE I. Hole mobilities (in cm^2 V^{-1} s^{-1}) obtained by velocity averaging for ideal and equilibrated morphologies. In the 1D case only coupling between nearest neighbors along the column is taken into account, while in the 3D case intercolumnar transport is allowed. FC stands for the fully conjugated model, while SM denotes the model with a single monomer as a conjugated segment.

	Direction	1D	3D (FC)	3D (SM)
Ideal lattice	x	⋯	0.187	0.573
	y	⋯	0.200	0.550
	z	1.2×10^{-3}	0.366	1.839
Equilibrated	x	⋯	1.195	0.566
	y	…	1.176	0.556
	z	0.052	0.465	1.165
Equilibrated + $\Delta G_{ij}^{\text{estat}}$	x	⋯	0.648	0.074
	y	⋯	0.686	0.121
	z	0.039	0.261	0.240

Hole mobilities are calculated by averaging the charge carrier velocity along the field direction for 10^{-7} s. Three cases are considered: an ideal configuration (i), the equilibrated system with (ii) and without (iii) electrostatic contributions. In the former case, the rings as optimized in vacuum were stacked into hexagonally ordered columns with a rotation of neighboring molecules by 30° with respect to each other. KMC runs were averaged for 100 different starting positions. For the equilibrated systems, charge mobility was calculated based on the last 100 frames of the MD production run with ten different starting positions per frame. Note that the system size is rather small in the x and y directions (4×4 hopping sites). However, intercolumnar hops occur along the whole length of the columns which improves averaging in the x and y directions. The resulting hole mobilities for 1D and 3D transport are summarized in Table I.

For both 1D and 3D transport, the calculated mobilities of the ideal system are lower than those obtained for the equilibrated morphology. This can be explained by the nonplanar conformation of the individual macrocycles as resulting from the DFT-based optimization in vacuum. Combined with the helical pitch of the stacking, this leads to a reduced overlap of the molecular orbitals which determine the transfer integral. In the equilibrated morphology, individual carbazole segments can reorient and overall consecutive cycles appear to align in a fashion that increases the electronic coupling, which results in the higher hole mobility. For the 1D

case, we additionally find large variations of the calculated mobilities for different snapshots due to the importance of pairs with low transfer integrals as is already known, e.g., for hexabenzocoronene or perylenediimide.[13,15,34,35]

Taking the three-dimensionality of the transporting network into account increases charge mobility along the column by one order of magnitude (from 0.05 to 0.5 $cm^2/V\,s$) for the equilibrated system and differences in mobilities between frames become negligible. The improvement is due to the fact that in three dimensions the additional pathways allow for defects in a column to be circumvented. Thus, the low transfer integrals in a column no longer prevent transport. It is noteworthy that the hole mobility within the *xy* plane is of the same order of magnitude than in the *z*-direction. This is a result of the high coupling due to the alignment of monomer segments, as shown in Fig. 1(d), and the large hopping distance of about 4 nm within the *xy* plane in the fully conjugated model or high velocity along the polymer chain in the single monomer model.

Energetic disorder is known to decrease the mobility by several orders of magnitude in compounds with a strong dipole moment.[36] In the present case, however, electrostatic disorder leads to a reduction of mobility by merely a factor of 2 in both one- and three-dimensional simulations as well as in all directions (for example, from 0.47 to 0.26 $cm^2/V\,s$ in the *z*-direction in 3D). This indicates that in the equilibrated morphology, the changes of the conformation of the individual macrocycles do not result in a significant increase of their dipole moment compared to their optimized vacuum conformation.

IV. SUMMARY

By combining molecular dynamics and kinetic Monte Carlo simulations, we have studied the charge transport properties of a columnar mesophase of carbazole macrocycles. We have shown that this system allows charge transport in three dimensions due to inward-facing side chains. The intercolumnar transport leads to an increase in mobility by at least an order of magnitude compared to solely intracolumnar transport because it helps to circumvent neighbors with low couplings along a column. For such a supramolecular arrangement, local mobilities are expected to be on the order of 0.1 $cm^2/V\,s$. Most importantly, this system is almost insensitive to local defects due to the three-dimensional nature of the charge percolation network.

ACKNOWLEDGMENTS

This work was partially supported by DFG via IRTG program between Germany and Korea, Grant Nos. AN 680/1-1 and SPP1355, and the BMBF program MESOMERIE. D.A. acknowledges the Multiscale Materials Modeling Initiative of the Max Planck Society. We thank Mara Jochum, Victor Rühle, Alexander Lukyanov, Falk May, Manuel Schrader, and Null Komma Josef for critical reading of the manuscript.

[1] K. M. Coakley and M. D. McGehee, Chem. Mater. **16**, 4533 (2004).
[2] P. W. M. Blom, V. Mihailetchi, L. Koster, and D. Markov, Adv. Mater. (Weinheim, Ger.) **19**, 1551 (2007).
[3] C. W. Tang, Appl. Phys. Lett. **48**, 183 (1986).
[4] G. A. Buxton and N. Clarke, Phys. Rev. E **74**, 041807 (2006).
[5] V. Coropceanu, J. Cornil, D. A. da Silva Filho, Y. Olivier, R. Silbey, and J.-L. Bredas, Chem. Rev. (Washington, D.C.) **107**, 926 (2007).
[6] A. Troisi, Adv. Mater. (Weinheim, Ger.) **19**, 2000 (2007).
[7] D. L. Cheung and A. Troisi, Phys. Chem. Chem. Phys. **10**, 5941 (2008).
[8] N. Vukmirović and L.-W. Wang, Phys. Rev. B **81**, 035210 (2010).
[9] L. Schmidt-Mende, A. Fechtenkotter, K. Müllen, E. Moons, R. H. Friend, and J. D. MacKenzie, Science **293**, 1119 (2001).
[10] V. Lemaur, D. A. da Silva Filho, V. Coropceanu, M. Lehmann, Y. Geerts, J. Piris, M. G. Debije, A. M. van de Craats, K. Senthilkumar, L. D. A. Siebbeles, J. M. Warman, J.-L. Brédas, and J. Cornil, J. Am. Chem. Soc. **126**, 3271 (2004).
[11] Y. Olivier, L. Muccioli, V. Lemaur, Y. H. Geerts, C. Zannoni, and J. Cornil, J. Phys. Chem. B **113**, 14102 (2009).
[12] E. Di Donato, R. P. Fornari, S. Di Motta, Y. Li, Z. Wang, and F. Negri, J. Phys. Chem. B **114**, 5327 (2010).
[13] J. Kirkpatrick, V. Marcon, J. Nelson, K. Kremer, and D. Andrienko, Phys. Rev. Lett. **98**, 227402 (2007).
[14] V. Marcon, T. Vehoff, J. Kirkpatrick, C. Jeong, D. Y. Yoon, K. Kremer, and D. Andrienko, J. Chem. Phys. **129**, 094505 (2008).
[15] J. Kirkpatrick, V. Marcon, K. Kremer, J. Nelson, and D. Andrienko, J. Chem. Phys. **129**, 094506 (2008).
[16] X. Feng, V. Marcon, W. Pisula, M. Hansen, J. Kirkpatrick, F. Grozema, D. Andrienko, K. Kremer, and K. Müllen, Nature Mater. **8**, 421 (2009).
[17] S.-S. Sun, C. Zhang, A. Ledbetter, S. Choi, K. Seo, and J. C. E. Bonner, Appl. Phys. Lett. **90**, 043117 (2007).
[18] S. King, M. Sommer, S. Huettner, M. Thelakkat, and S. A. Haque, J. Mater. Chem. **19**, 5436 (2009).
[19] S.-H. Jung, W. Pisula, A. Rouhanipour, H. J. Räder, J. Jacob, and K. Müllen, Angew. Chem., Int. Ed. **45**, 4685 (2006).
[20] B. Schmaltz, A. Rouhanipour, H. J. Räder, W. Pisula, and K. Müllen, Angew. Chem., Int. Ed. **48**, 720 (2009).
[21] B. Hess, C. Kutzner, D. van der Spoel, and E. Lindahl, J. Chem. Theory Comput. **4**, 435 (2008).
[22] T. Vehoff, J. Kirkpatrick, K. Kremer, and D. Andrienko, Phys. Status Solidi B **245**, 839 (2008).
[23] U. Essmann, L. Perera, M. L. Berkowitz, T. Darden, H. Lee, and L. G. Pedersen, J. Chem. Phys. **103**, 8577 (1995).
[24] G. Bussi, D. Donadio, and M. Parrinello, J. Chem. Phys. **126**, 014101 (2007).
[25] V. Rühle, C. Junghans, A. Lukyanov, K. Kremer, and D. Andrienko, J. Chem. Theory Comput. **5**, 3211 (2009).
[26] V. Rühle, J. Kirkpatrick, and D. Andrienko, J. Chem. Phys. **132**, 134103 (2010).
[27] R. A. Marcus, Rev. Mod. Phys. **65**, 599 (1993).
[28] K. F. Freed and J. Jortner, J. Chem. Phys. **52**, 6272 (1970).
[29] M. J. Frisch, G. W. Trucks, H. B. Schlegel *et al.*, GAUSSIAN 03, Revision B.05, Gaussian, Inc., Pittsburgh, PA, 2003.
[30] P. J. Stephens, F. J. Devlin, C. F. Chabalowski, and M. J. Frisch, J. Phys. Chem. **98**, 11623 (1994).
[31] J. Kirkpatrick, Int. J. Quantum Chem. **108**, 51 (2008).
[32] B. Baumeier, J. Kirkpatrick, and D. Andrienko, Phys. Chem. Chem. Phys. **12**, 11103 (2010).
[33] T. Vehoff, B. Baumeier, A. Troisi, and D. Andrienko, J. Am. Chem. Soc. **132**, 11702 (2010).
[34] D. Andrienko, V. Marcon, and K. Kremer, J. Chem. Phys. **125**, 124902 (2006).
[35] V. Marcon, D. W. Breiby, W. Pisula, J. Dahl, J. Kirkpatrick, S. Patwardhan, F. Grozema, and D. Andrienko, J. Am. Chem. Soc. **131**, 11426 (2009).
[36] S. Novikov, D. Dunlap, V. Kenkre, P. Parris, and A. Vannikov, Phys. Rev. Lett. **81**, 4472 (1998).